

Differentiation of mass-forming focal pancreatitis from pancreatic ductal adenocarcinoma: value of characterizing dynamic enhancement patterns on contrast-enhanced MR images by adding signal intensity color mapping

Mimi Kim¹ · Kyung Mi Jang^{2,3} · Jae-Hun Kim² · Woo Kyoung Jeong² · Seong Hyun Kim² · Tae Wook Kang² · Young Kon Kim² · Dong Ik Cha² · Kyunga Kim⁴

Received: 3 January 2016 / Revised: 18 July 2016 / Accepted: 20 July 2016 / Published online: 10 August 2016
© European Society of Radiology 2016

Abstract

Objectives To evaluate the value of dynamic enhancement patterns on contrast-enhanced MR images by adding signal intensity colour mapping (SICM) to differentiate mass-forming focal pancreatitis (MFFP) from pancreatic ductal adenocarcinoma (PDAC).

Methods Forty-one clinicopathologically proven MFFPs and 144 surgically confirmed PDACs were enrolled. Laboratory and MR imaging parameters were used to differentiate MFFP from PDAC. In particular, enhancement patterns on MR images adding SICM were evaluated. By using classification tree analysis (CTA), we determined the predictors for the differentiation of MFFP from PDAC.

Results In the CTA, with all parameters except enhancement pattern on SICM images, ductal obstruction grade and T1 hypointensity grade of the pancreatic lesion were the first and second splitting predictor for differentiation of MFFP from PDAC, in order. By adding an enhancement pattern on

the SICM images to CTA, the enhancement pattern was the only splitting predictor to differentiate MFFP from PDAC. The CTA model including enhancement pattern on SICM images has sensitivity of 78.0 %, specificity of 99.3 %, and accuracy of 94.6 % for differentiating MFFP from PDAC.

Conclusion The characterization of enhancement pattern for pancreatic lesions on contrast-enhanced MR images adding SICM would be helpful to differentiate MFFP from PDAC.

Key Points

- SICM was useful to characterize enhancement pattern.
- Enhancement pattern on SICM was the only splitting predictor on CTA.
- This model may be useful for differentiating MFFP from PDAC.

Keywords Pancreatic ductal adenocarcinomas · Mass-forming focal pancreatitis · Magnetic resonance imaging · Signal intensity colour mapping · Classification tree analysis

✉ Kyung Mi Jang
kmmks.jang@samsung.com

¹ Department of Radiology, Hanyang Medical Center, Hanyang University College of Medicine, Seoul, Republic of Korea

² Department of Radiology, Samsung Medical Center, Sungkyunkwan University School of Medicine, Seoul, Republic of Korea

³ Department of Radiology and Center for Imaging Science, Samsung Medical Center, Sungkyunkwan University School of Medicine, 50 Irwon-Dong, Gangnam-gu, Seoul 135-710, Korea

⁴ Biostatistics and Clinical Epidemiology Center, Research Institute for Future Medicine, Samsung Medical Center, Seoul, Republic of Korea

Abbreviations

PDAC	Pancreatic ductal adenocarcinomas
MFFP	Mass-forming focal pancreatitis
CBD	Common bile duct
MPD	Main pancreatic duct
SICM	Signal intensity colour mapping
MR	Magnetic resonance
DWI	Diffusion-weighted imaging
ADC	Apparent diffusion coefficient
CTA	Classification tree analysis

Table 1 Demographic and clinical characteristics

Parameter	MFFP	PDAC
No. of patients	41	144
Mean age (years)	61.5	65.6
Age range (years)	46-80	33-88
No. of men	31	81
Mean age (years)	64.1	62.9
Age range (years)	47-83	40-88
No. of women	10	63
Mean age (years)	56.8	64.5
Age range (years)	22-75	35-80
Mean follow-up (months)	21.5	–
Range of follow-up (months)	17-39	–
Diagnosis		
Autoimmune, IgG4 type	17	–
Autoimmune, unspecified	13	–
Chronic pancreatitis	8	–
Acute focal pancreatitis	3	–
Site in the pancreas		
Head	21	94
Neck	1	4
Body	4	23
Tail	15	23
Size (mm)		
Mean	33	28
Range	12-79	9-63
Amylase elevation	16	27
Lipase elevation	22	63
CA19-9 elevation	5	94

Note: MFFP = mass-forming focal pancreatitis, PDAC= pancreas ductal adenocarcinoma, CA19-9 = carbohydrate antigen 19-9

Introduction

Accurately differentiating between pancreatic ductal adenocarcinoma (PDAC) and mass-forming focal pancreatitis (MFFP) is important because their prognosis and management are quite different [1, 2]. However, in cases of a focal form of autoimmune pancreatitis, which may present as a focal mass in the pancreas with obstruction of the common bile duct (CBD) or main pancreatic duct (MPD), it has been difficult to differentiate them from PDAC on cross-sectional imaging studies, and many patients with MFFP have undergone unnecessary pancreatic resections [3–6].

On pathology, the typical feature of PDAC is complete disappearance of pancreas parenchyma due to carcinogenesis and desmoplasia (abundant fibrotic stroma) [7–9]. As the areas of progressive enhancement within the mass-forming intrahepatic cholangiocarcinoma correspond to desmoplastic stroma due to pooling of contrast material [10], desmoplastic stroma of PDAC might also appear as the dominant

Table 2 MR Imaging Sequences and Parameters

Sequence	TR/TE (ms)	Flip angle (°)	Section thickness (mm)	Matrix size	Bandwidth (Hz/pixel)	Field of view (cm)	Acquisition time (s)	No. of Excitations
T1W 3D dual GRE	3.5/1.15-2.3	10	6	288 × 230	434.4/0.243	32-38	14	1
T1W 3D GRE	31-1.5	10	2	256 × 256	955.7/0.601	32-38	16.6	1
BH-MS-T2WI	2161/70	90	5	324 × 235	235.2/1.702	32-38	55	1
RT-SS-HT2WI	1573/160	90	5	320 × 256	317.9/1.117	32-38	120	2
BH-2D-MRCP	6417/921	90	40	256 × 256	438.2/0.992	25	3	1
NT-3D-MRCP	1673/650	90	2	320 × 206	662.9/0.655	35	180-240	2
DWI	1600/70	90	5	112 × 108	79.5/5.467	34	126	4

Note: TR (repetition time), TE (echo time), 3D (three-dimensional), GRE (gradient echo), BH-MS-T2WI (Breath-hold multi-shot T2 weighted imaging), RT-SS-HT2WI (Respiratory-triggered single-shot heavily T2 weighted imaging), BH-2D-MRCP (Breath-hold two-dimensional single-projection MR cholangiopancreatography), NT-3D-MRCP (Navigator-triggered three-dimensional MR cholangiopancreatography)

hypovascular solid portion on arterial phase images and would show progressive enhancement as it goes from arterial to delayed phase images. In contrast, in MFFP, the pancreatic parenchyma is not totally replaced by fibrosis, and acinar cells are preserved [11, 12]. Therefore, the enhancement pattern of MFFP would be different from that of PDAC. Accordingly, we thought that the characterization of the hypovascular portion in the pancreatic lesions on contrast-enhanced MR images would be important to differentiate between MFFP and PDAC. And we thought that adding signal intensity colour mapping (SICM) to greyscale dynamic MR images would be helpful to determine the dominant hypovascular solid portion of the pancreatic lesions on arterial phase image and to characterize the enhancement pattern of the pancreatic lesions because of the colour contrast.

Accordingly, the purpose of this study was to determine the value of enhancement patterns on contrast-enhanced MR images by adding SICM to differentiate MFFP from PDAC.

Material and methods

Study population

This retrospective study was approved by our institutional review board and the requirement for informed consent was waived. To constitute the MFFP group of this study, we searched our institutional radiologic MR imaging database using the search term “pancreatitis” between July 2008 and May 2015. Then, those who met the following inclusion criteria were selected: (a) patients with clinicopathologically proven pancreatitis with no evidence of malignancy; (b) patients who underwent pancreas MR imaging according to our standard protocol for diagnosis of pancreatic lesions; (c) patients with mass-forming lesion, which was defined as a lesion distinguishable from the adjacent pancreas parenchyma because of abnormal signal intensity or a focal lesion with localized bulging contour of the pancreas on unenhanced T1-

Table 3 Assessed MR Imaging Parameters and Its Definitions

Parameters	Definition
Margin of the lesion	Distinct versus Indistinct
Peripancreatic capsule-like rim	Hypointensity surrounding the pancreatic lesion on both T1- and T2-weighted images, showed delayed enhancement
Vascular involvement of the lesion	Grade 1, No involvement Grade 2, Abutting equal to or less than 90 degrees of the vessel circumference Grade 3, Abutting more than 90 degrees of the vessel circumference with no or mild luminal change Grade 4, Abutting more than 90 degrees of the vessel circumference with angular border, stenosis or occlusion
Hypointensity of the lesion on T1WI	Grade 1, lesion \geq spleen Grade 2, renal medulla < lesion < spleen Grade 3, lesion \leq renal medulla
Signal intensity of the lesion on DWI	Grade 1, lesion \leq adjacent pancreas Grade 2, adjacent pancreas < lesion < spleen Grade 3, lesion \geq spleen
Appearances of the lesion on T2WI	Type 1, solid Type 2, intratumoral unilocular cyst Type 3, intratumoral multifocal cystic foci
MPD obstruction	Grade 1, no obstruction Grade 2, non-obstructed, but narrowed MPD penetrating the mass Grade 3, complete obstruction with icicle or ice pick feature Grade 4, complete obstruction without icicle or ice pick feature
CBD obstruction	Grade 1, no obstruction Grade 2, non-obstructed, but narrowed CBD penetrating the mass Grade 3, smoothly tapered complete obstruction Grade 4, not smoothly tapered complete obstruction
*Signal intensities of the lesion on contrast-enhanced MR images	Type 1, hypointense-isointense-iso, or hyperintense Type 2, hypointense-hypointense-iso, or hyperintense Type 3, hypointense-hypointense-hypointense Type 4, hypointense-target feature on portal or delayed images Type 5, unclassifiable enhancement

* Signal intensities of the lesion on arterial, portal, and 3-min late phase images, using the adjacent normal pancreatic parenchyma as a reference. Target feature means the lesion has a more hyperintense solid peripheral region surrounding a more hypointense central solid region.

T1WI = T1-weighted images, DWI = diffusion-weighted images, T2WI = T2-weighted images MPD = main pancreatic duct, CBD = common bile duct

weighte images (T1WI) or contrast-enhanced MR images[2]. We excluded diffuse or multifocal forms of pancreatitis. A total of 41 consecutive patients were included in the MFFP group. All patients underwent pancreas MRI within 1 month (mean, 12 days; range, 3–28 days) prior clinicopathologic diagnosis of pancreatitis. The diagnosis of MFFP was established based on the following clinicopathology results: (a) surgical resection (n=14); (b) endoscopic ultrasound guided biopsy (n=25); (c) spontaneous resolution without biopsy (n=2) on follow-up imaging.

For the PDAC group of this study, we searched our institutional surgicopathology database using the search terms “pancreas cancer” and “pancreas ductal adenocarcinoma” between January 2014 and March 2015. Then, those who met the following inclusion criteria were selected: (a) patients who underwent pancreas MR imaging within 1 month prior to surgery according to our standard protocol; (b) no imaging features of diffuse involvement, distant metastasis or peritoneal seeding. Among them, four patients with motion artefact were excluded. A total of 144 consecutive patients were included in the PDAC group.

Review of pathology reports and MR images to determine the eligibility for enrolment for this study was performed by one abdominal radiologist (W.K.J. with 10 years of experience in abdominal MR imaging interpretation). He also recorded the location and size of the pancreatic lesions on MRI and whether serum levels of amylase, lipase, and carbohydrate antigen 19-9 (CA 19-9) of the patients were elevated during the period of hospitalization for diagnosis of pancreatic lesions. At our institution, the definition of elevated amylase, lipase, and CA 19-9 are serum levels higher than 100U/L, 60U/L, and 37U/mL, respectively. Clinical and demographic data of the MFFP and PDAC groups are summarized in Table 1.

MR imaging technique

All MR images were acquired using a 3.0-T MR system (Intera Achieva 3.0-T, Philips Healthcare, Best, the Netherlands) with a 16-channel phased-array receiver coil. MRI sequences are summarized in Table 2. Dynamic enhancement imaging studies were obtained using a T1-weighted 3-dimensional turbo-field-echo sequence with a spectral attenuated inversion-recovery fat-suppression technique and included unenhanced phase, arterial-phase (20–35 s), portal phase (60 s), late phase (3 min), and 20 min hepatobiliary phase. For enhancement study, gadoteric acid was used as a contrast agent (Primovist; Bayer Schering Pharma, Berlin, Germany). Using a power injector, the contrast agent was applied intravenously at a rate of 2 mL/s for a dose of 0.025 mmol/kg body weight, followed by a 20-mL saline flush. The time for the arterial phase imaging was determined using the MR fluoroscopic bolus detection technique [13].

For evaluation of pancreatic and bile duct anatomy, we used two different MR cholangiopancreatography (MRCP) methods. Sequence parameters for MRCP were optimized by vendor according to protocols. A breath-hold 2D single-projection turbo spin-echo MRCP and a navigator-triggered 3D MRCP were acquired sequentially.

Diffusion-weighted (DW) imaging with a b -value of 0, 100, and 800 s/mm^2 were acquired before the administration of contrast agent using a respiratory-triggered single-shot echo planar imaging. The spectral presaturation with inversion recovery was used for fat suppression. The beginning of each acquisition was timed to the same state of the respiratory cycle. The apparent diffusion coefficient (ADC) was calculated with a monoexponential function using b -values of 100 and 800 s/mm^2 .

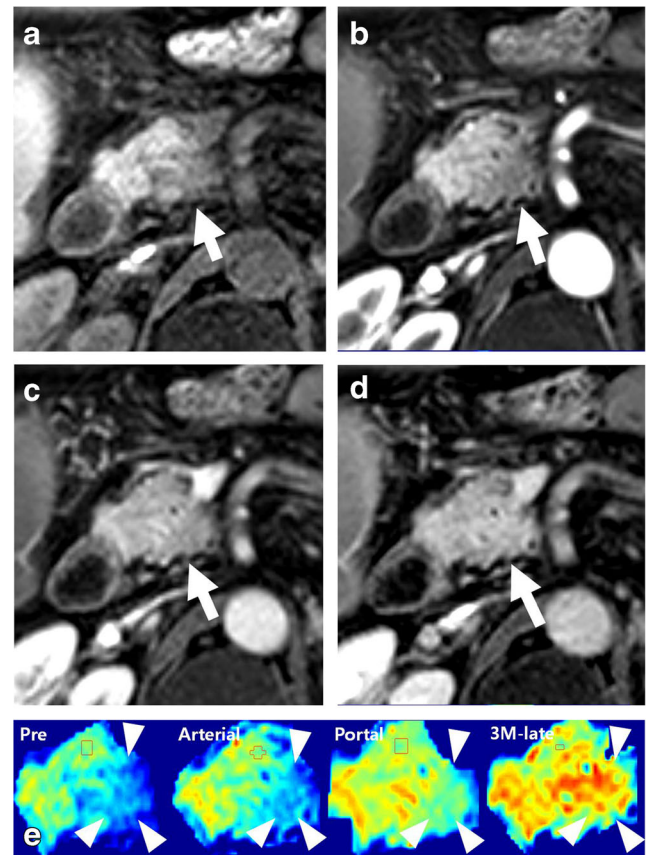


Fig. 1 Pancreatic ductal adenocarcinoma developed in the pancreas uncinata process in a 54-year-old man. On transverse unenhanced T1-weighted (a) and arterial phase (b) images, the lesion (arrows) shows ill-defined area of hypointensity. On the portal (c) and 3-min late phase (d) images, the lesion (arrows) shows mild homogeneous hypointensity and hyperintensity compared with adjacent pancreas parenchyma, respectively. The lesion (arrows) shows progressive enhancement toward the dominant hypovascular foci (arrowheads) on signal intensity colour mapping images (e) of arterial, portal and 3-min late phase images

Acquisition of SICM

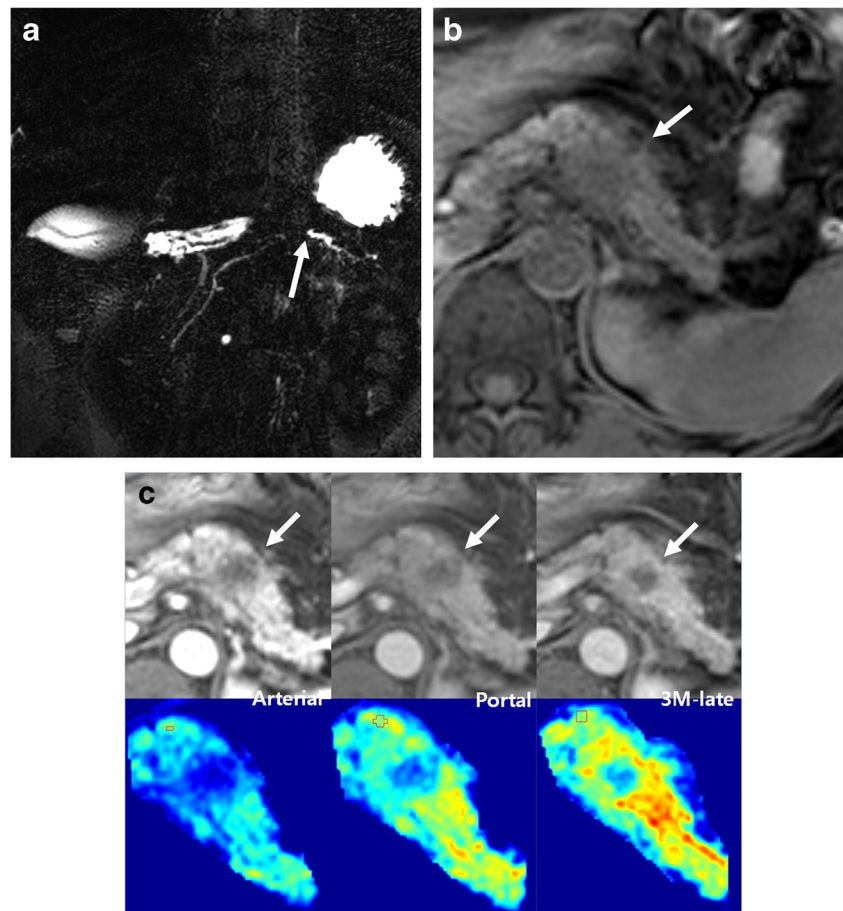
Data for unenhanced, arterial, portal, and 3-min late MR images were transferred to a personal computer workstation and analyzed for SICM using in-house software written using MATLAB v. 7.6 (Mathworks, Natick, MA, USA). For SICM of the lesion, we set up the reference point as normal pancreas parenchyma near the lesion on each phase. ROI of reference point was determined by two radiologists (S.H.K. and W.K.J. with 15 and 10 years of experience, respectively) on consensus. We described the ROI of a reference point on each phase (arterial, portal, and 3 min late phase) at the same location as the ROI on the unenhanced image by side-by-side comparison. The percent signal change was computed as
$$\text{The percent signal change} = \frac{(\text{lesion signal intensity} - \text{reference signal intensity})}{\text{reference signal intensity}} \times 100.$$
 The percent signal change was mapped onto a colour image from blue to red. For example, when the lesion showed lower signal intensity than the reference point of normal parenchyma, the colour of the lesion was changed from yellow-green to blue depending on the signal intensity difference between the lesion and reference point of normal parenchyma. On the other hand, when the lesion showed higher signal intensity than normal parenchyma, the colour of the lesion changed from yellow-green to red depending on the signal intensity

difference between the lesion and reference point of normal parenchyma. The minimum and maximum of colour scale was set as -80 % and 80 % arbitrary.

Imaging analysis

All MR images were evaluated by two abdominal radiologists (K.M.J. and T.W.K. with 14 and 6 years of experience, respectively, in abdominal MR imaging interpretation) in consensus on a picture archiving and communication system (Pacs; GE Medical Systems Integrated Imaging Solutions, Mt. Prospect, IL, USA), with an adjustment of the optimal window setting in each case. These readers were unaware of the clinicopathological diagnoses of pancreatic lesions. In cases of disagreement, a third reader (Y.K.K. with 15 years of experience in abdominal MRI) was asked for an opinion and the majority opinion was used for data analysis. At first, readers evaluated the MR imaging features listed in Table 3, which were reported with regard to the imaging features of PDAC and MFPF on previous reports [1, 2, 14–19]. Then, the readers classified the enhancement pattern of the lesion on dynamic MR images with adding SICM. Firstly, the readers determined the dominant hypovascular foci in the pancreatic lesion on arterial SICM images (Figs. 1 and 2). Secondly, the

Fig. 2 Pancreatic ductal adenocarcinoma developed in the pancreas uncinata process in a 53-year-old woman. MR cholangiopancreatography (a) shows a grade 4 ductal obstruction, abrupt cut-off the upstream main pancreatic duct with tortuosity. On transverse unenhanced T1-weighted image (b), the lesion (arrow) shows hypointensity compared to the spleen. On arterial, portal and 3-min late phase (c) images, the lesion (arrows) shows ill-defined area of hypointensity. The lesion shows progressive centripetal enhancement on signal intensity colour mapping images (c, bottom line) of arterial, portal and 3-min late phase images



enhancement patterns of the pancreatic lesions on SICM images were classified as follows: (1) pattern 1, progressive enhancement toward the dominant hypovascular foci in the lesion (Figs. 1 and 2); (2) pattern 2, persistent hypovascularity with no incremental enhancement; (3) pattern 3, sudden homogeneous enhancement of the lesion on portal or delayed SICM images (Fig. 3); (4) pattern 4, unclassifiable hypovascular enhancement (Fig. 4); (5) pattern 5, hypervascular enhancement.

For quantitative analysis, readers measured ADC and normalized ADC values of the lesions on the ADC map by using manually defined circular or ovoid regions of interest (mean, 1.15 mm^2 ; range, $6.3\text{--}200.0 \text{ mm}^2$) on the pancreatic lesions and adjacent paravertebral muscle. The spatial cursor key in the PACS that enabled matching of the corresponding sites on different images was used. Each value was obtained for the solid component of lesions using the largest possible circle or oval while avoiding cystic areas. The ADC values were recorded as the average of three separately measured regions of interest on each image. The ADC value of the paravertebral muscle was used for the normalization of ADC values [20]

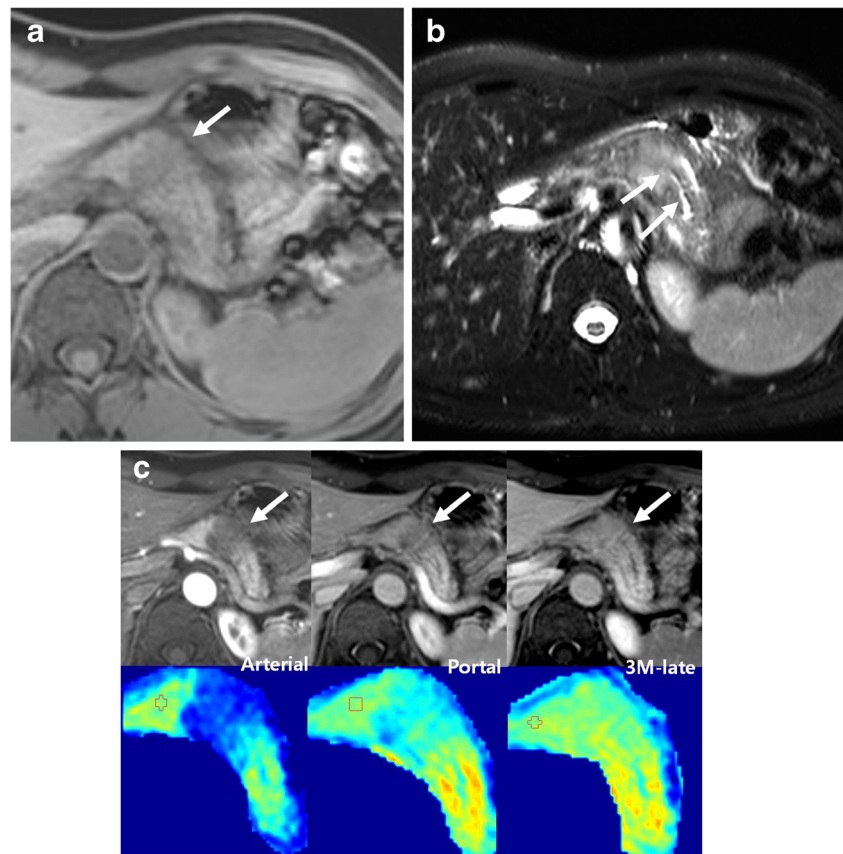
Statistical analysis

Laboratory and MR imaging parameters were analyzed via univariate logistic regression to investigate their

association with MFFP. For each parameter, odd ratio (OR) of MFFP against PDAC was provided with its 95 % confidence interval. Firth's penalized maximum likelihood estimation method was applied to logistic regression when categorical parameters showed cell sparsity. The grade of ductal obstruction was defined as a higher value between grades of MPD and CBD. The Student's t-test was performed to compare the ADC value and normalized ADC value between MFFP vs. PDAC groups.

Classification tree analyses (CTAs) were performed to identify predictors for MFFP and derive simple classification algorithms that differentiate MFFP from PDAC: CTA with all parameters except enhancement pattern on SICM images and CTA including enhancement pattern on SICM images. Decision tree and random forest methods were used for CTAs [21] with packages "rpart" and "randomForest" in R 3.2.1 (Vienna, Austria; <http://www.R-project.org/>). We selected final classification models, which showed the least cross-validation error and had proper numbers of patients in terminal nodes. Performances of the final models were evaluated and compared based on accuracy, sensitivity, specificity, positive predictive value (PPV), and negative predictive value (NPV). All the other statistical analysis was executed using SAS version 9.4 (SAS Institute Inc, Cary, NC, USA). All p -values < 0.05 were considered to be statistically significant.

Fig. 3 Autoimmune pancreatitis developed in the pancreas body in a 47-year-old woman. On transverse unenhanced T1-weighted image (a), the lesion (arrow) shows similar intensity to that of the spleen. On transverse heavily T2-weighted image (b), the main pancreatic duct (arrowheads) is smoothly narrowed by the lesion (arrows). On the arterial and portal phase images (c), the lesion (arrowheads) shows ill-defined area of hypointensity. On the 3-min late phase image (c), the lesion shows homogeneous enhancement. The lesion (arrows) shows sudden homogeneous enhancement on signal intensity colour mapping image (c, bottom line) of 3-min late phase



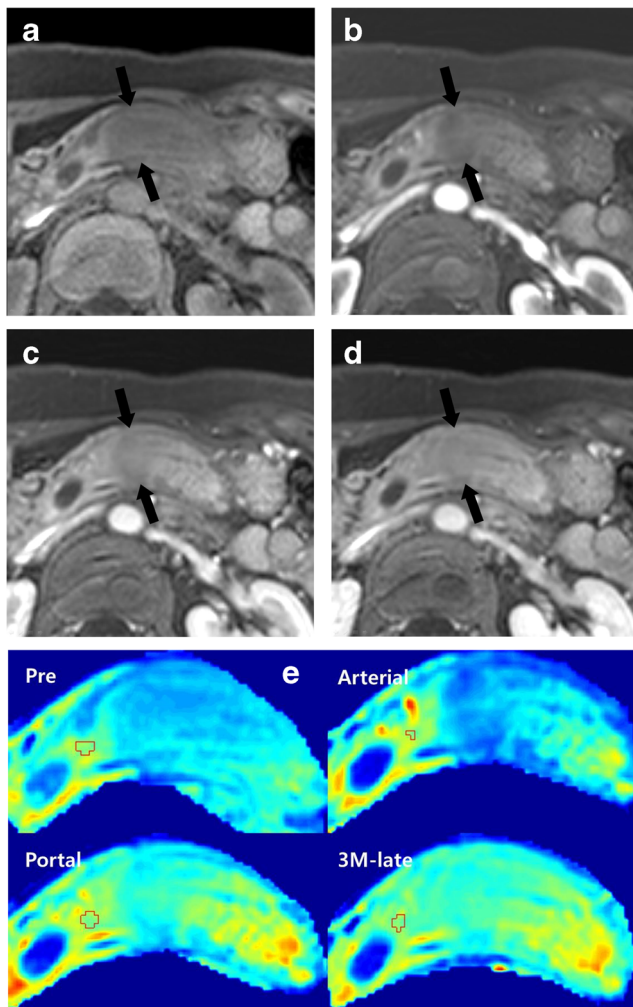


Fig. 4 Autoimmune pancreatitis developed in the pancreas body in a 48-year-old man. On transverse unenhanced T1-weighted (a), arterial (b), portal (c), and 3-min late phase (d) images, the lesion (arrows) shows persistent and mild hypovascular enhancement compared to the adjacent pancreas without progressive enhancement toward the dominant hypovascular foci on signal intensity colour mapping images (e) of unenhanced, arterial, portal and 3-min late phase images

Results

The laboratory and MR imaging parameters of both groups are summarized in Table 4. Among assessed laboratory and MR imaging parameters, the following parameters were significantly associated with MFFPs: amylase elevation, peripancreatic capsule-like rim, grade 1 hypointensity on T1-weighted images, solid appearance on T2-weighted images, ductal obstruction grade equal to or less than 3, type 1 or 2 signal intensities on contrast-enhanced MR images, pattern 3 or 4 enhancement on SICM images ($p < 0.05$) (Figs. 3 and 4). However, only peripancreatic capsule-like rim was exclusively shown in MFFPs. Type 1 or 2 signal intensities on contrast-enhanced MR images was appeared in 22.3 % (32/144) of PDACs (Fig. 1), and pattern 3 enhancement on SICM images was appeared in 0.7 % (1/144) of PDACs. On

quantitative analysis, ADC and normalized ADC values were significantly different between the MFFP group and PDAC group (ADC values, [mean, $1.044 \pm 0.205 \times 10^{-3} \text{ mm}^2/\text{s}$; range, $0.717 - 1.580 \times 10^{-3} \text{ mm}^2/\text{s}$] versus [mean, $1.176 \pm 0.225 \times 10^{-3} \text{ mm}^2/\text{s}$; range, $0.419 - 1.953 \times 10^{-3} \text{ mm}^2/\text{s}$]; normalized ADC values [mean, 0.69 ± 0.14 ; range, $0.46 - 1.00$] versus [mean, 0.76 ± 0.14 ; range, $0.27 - 1.16$]) ($p < 0.05$).

The results of CTAs are shown in Fig. 5. In the first CTA with all parameters except enhancement pattern on SICM images, ductal obstruction grade and T1 hypointensity grade were the first and second splitting predictors for differentiation MFFP from PDAC group in order. Of 33 lesions with ductal obstruction grade equal to or less than 3 and grade 1 T1 hypointensity, 29 (87.9 %) lesions were MFFPs (Fig. 3). On the second CTA with adding enhancement pattern on SICM images, pattern 3 or 4 enhancement on SICM was the only predictor for the differentiation of MFFP group from PDAC group (Figs. 3 and 4). Of 33 lesions with pattern 3 or 4 enhancement on SICM images, 32 (97.0 %; pattern 3, $n=24$; pattern 4, $n=8$) lesions were MFFPs. Of remaining 152 lesions with pattern 1, 2, or 5 enhancements on SICM images, 143 (94.1 %; pattern 1, $n=137$; pattern 2, $n=3$; pattern 5, $n=3$) lesions were PDACs (Figs. 1 and 2). All 25 lesions with ductal obstruction grade equal to or less than 3, grade 1 T1 hypointensity, and pattern 3 or 4 enhancement on SICM images were all MFFPs. Six cases were more correctly assessed in differentiating between MFFP and PDAC using the second CTA compared with the first CTA. (Figure 1). Eleven cases (7 PDACs and 4 MFFPs) incorrectly classified in the first CTA were correctly diagnosed in the second CTA, and five cases (one PDAC and four MFFPs) correctly diagnosed in the first CTA were incorrectly classified in second CTA. The established classification tree models have sensitivity of 70.7 %, specificity of 97.2 %, PPV of 87.9 %, NPV of 92.1 %, and diagnostic accuracy of 91.4 % on the first CTA, and sensitivity of 78.0 %, specificity of 99.3 %, PPV of 97.0 %, NPV of 94.1 %, and diagnostic accuracy of 94.6 % on the second CTA for differentiation of MFFP from PDAC.

Discussion

On previous studies [17, 22–24], the characteristic enhancement appearances of MFFP have been described as homogeneous enhancement during the portal and late phases MR images. In this study, although similar enhancement appearances (i.e., type 1 and 2 signal intensities on contrast enhanced MR images in this study) were more frequently seen in MFFPs (78 %, 32/41), those types of enhancement were also seen in 22.3 % (32/144) of PDACs. However, by adding of SICM to contrast-enhanced MR images, which shows distinct

Table 4 Univariate Analysis for MR Imaging Parameters and Serologic Markers to Differentiate MFFP from PDAC

Parameter	MFFP (n=41)	PDAC (n=144)	OR	95 % CI of OR	p value
Amylase elevation*	16 (39.0)	27 (18.8)	0.36	0.17 - 0.77	0.008 [‡]
CA 19-9 elevation*	5 (12.2)	94 (65.3)	13.54	5.00 - 36.66	<.001 [‡]
Lipase elevation*	22 (53.7)	63 (43.8)	0.67	0.34 - 1.35	0.263
Margin of the lesion			1.85	0.60 - 5.68	0.282
Distinct	4 (9.8)	24 (16.7)			
Indistinct	37 (90.2)	120 (83.3)			
Peripancreatic capsule-like rim	6 (14.6)	0 (0.0)	0.02	0.01 - 0.43	0.013 [‡]
Vascular involvement of the lesion			1.17	0.89 - 1.53	0.272
Grade 1	19 (46.3)	65 (45.1)			
Grade 2	9 (22.0)	21 (14.6)			
Grade 3	5 (12.2)	7 (4.9)			
Grade 4	8 (19.5)	51 (35.4)			
Hypointensity of the lesion on T1WI			6.6	3.44 - 12.67	<.001 [‡]
Grade 1	32 (78.0)	31 (21.5)			
Grade 2	7 (17.0)	45 (31.3)			
Grade 3	2 (5.0)	68 (47.2)			
Signal intensity of the lesion on DWI			0.97	0.52 - 1.82	0.926
Grade 1	1 (2.5)	6 (4.2)			
Grade 2	13 (31.7)	42 (29.2)			
Grade 3	27 (65.8)	96 (66.6)			
Appearances of the lesion on T2WI					0.001 [‡]
Solid†	32 (78.0)	67 (46.5)
Unilocular	3 (7.3)	6 (4.2)	0.96	0.22 - 4.07	0.95
Multiple cystic foci	6 (14.7)	71 (49.3)	5.65	2.22 - 14.38	<.001 [‡]
Grade of ductal obstruction (MPD or CBD)°			1.68	1.35 - 2.09	<.001 [‡]
Grade 1	13 (31.7)	18 (12.5)			
Grade 2	4 (9.8)	1 (0.7)			
Grade 3	18 (43.9)	13 (9.0)			
Grade 4	6 (14.6)	112 (77.8)			
Signal intensities of the lesion on contrast-enhanced MR images			4.48	2.81 - 7.16	<.001 [‡]
Type 1	16 (39.0)	6 (4.2)			
Type 2	16 (39.0)	24 (16.7)			
Type 3	8 (19.5)	31 (21.5)			
Type 4	1 (2.5)	80 (55.5)			
Type 5	0 (0.0)	3 (2.1)			
Enhancement pattern on colour scale dynamic images			89.81	23.42 - 344.41	<.001 [‡]
Pattern 1	7 (17.0)	137 (95.1)			
Pattern 2	2 (5.0)	3 (2.1)			
Pattern 3	24 (58.5)	1 (0.7)			
Pattern 4	8 (19.5)	0 (0.0)			
Pattern 5	0 (0.0)	3 (2.1)			

Note. CI = confidence interval, OR = odds ratio, DWI = diffusion-weighted images, ADC = apparent diffusion coefficient, NA= not applicable. Data are number of lesions. Numbers in parentheses are percentages. The univariate logistic regression analysis was used to calculate p values. *Reference points: amylase - 100U/L, CA19-9 - 37 U/mL, lipase - 60 U/L. † Used as the reference category. °The higher grade was selected between grade of MPD and grade of CBD. ‡ Statistically significant results from logistic regression analysis.

contrast of the lesions, we could evaluate the dominant hypovascular portion and dynamic enhancement pattern of

pancreatic lesions more precisely. Only one case with PDAC showed pattern 3 enhancement on SICM images. The tumour

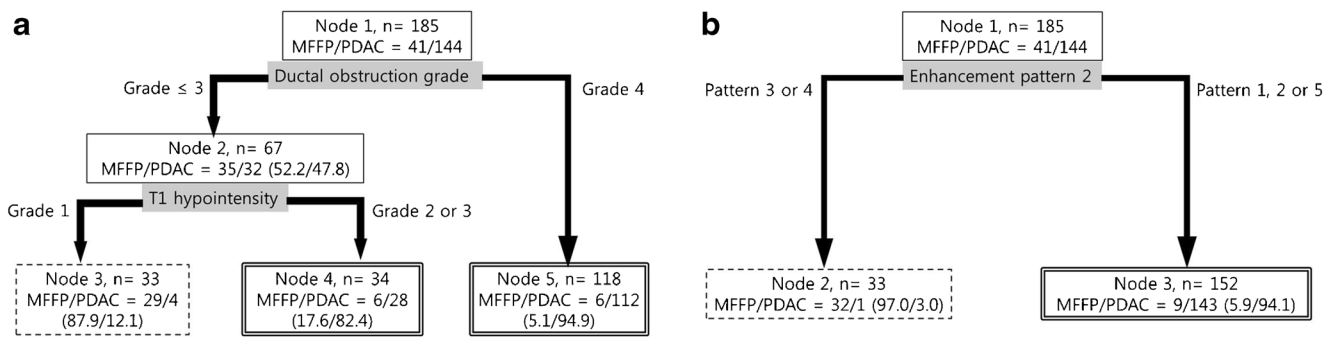


Fig. 5 Subgroups of the tumours identified through classification tree analysis and their risks to develop each groups. The schematic chart of (a) shows the results of classification tree analysis with all assessed parameters except enhancement pattern on signal intensity colour mapping images. The schematic chart of (b) shows the results of classification tree analysis with all assessed parameters including

had a well to moderately differentiated component in more than 95 % of the tumour, and less than 5 % of tumour had poorly differentiated component with minimal desmoplastic stromal reaction. As a result, the enhancement pattern on SICM was chosen as the only predictor to differentiate MFFP from PDAC on CTA. The enhancement differences between MFFP and PDAC were caused by the following pathological differences: complete disappearance of pancreatic parenchyma by carcinogenesis and desmoplasia (abundant fibrotic stroma) in PDAC and the infiltrative nature of inflammatory cells, mild interstitial fibrosis, and preserved acinar cells in MFFP [1, 16]. The dominant hypovascular portion in PDACs may represent the prominent fibrotic stroma.

In this study, ductal obstruction grade equal to or less than 3 and grade 1 T1 hypointensity were the first and second splitting predictors for differentiating MFFP from PDAC on the first CTA, and is in line with previous studies [16, 22, 23]. The different degree of duct obstruction in MFFP and PDAC was explained as follows: PDACs arise from the ductal epithelium and grow centrifugally, resulting in early complete ductal obstruction, whereas ductal stricture in MFFP is usually caused by centripetal narrowing by mass effect of periductal inflammation [25, 26]. Grade 1 T1 hypointensity in MFFP might be attributed to the preserved cellular components of the pancreas [16].

In this study, ADC values and normalized ADC values were significantly lower in the MFFP group than in PDAC group (mean, 1.044 ± 0.205 versus $1.176 \pm 0.225 \times 10^{-3} \text{ mm}^2/\text{s}$; 0.69 ± 0.14 versus 0.76 ± 0.14), which are in line with a previous study [27]. However, in other studies, the ADC values were significantly higher in MFFP than in PDAC [17, 28]. Additionally, apparent diffusion coefficients (ADCs) for pancreatic lesions could show marked variations depending on imaging sequences, the specific b values used for ADC calculation, or technical parameters of the data acquisition [29]. On the other hand, perfusion fraction f of intravoxel incoherent motion DW imaging has been reported as a better DW imaging-derived

enhancement pattern on signal intensity colour mapping. Data are number of lesions. Number in parentheses are percentages. Boxes with dotted line = the subgroup with high probability of a tumour to be MFFP; Boxes with bold double-line = the subgroup with high probability of a tumour to be PDAC

parameter for differentiating MFFP from PDACs than ADC values on previous studies [30, 31]. In these studies, the perfusion fraction f was significantly lower in carcinoma tissues than in inflammatory pancreatic lesions.

Misdiagnosing PDAC is associated with dismal prognosis and, therefore, the highest specificity possible should be achieved [32]. In this study, by using ductal obstruction grade and grade of T1 hypointensity on the first CTA, the specificity was 97.2 %. After adding the characterization of enhancement pattern on SICM imaging to CTA, the specificity was 99.3 %, and all 25 lesions with ductal obstruction grade equal to or less than 3, grade 1 T1 hypointensity and pattern 3 or 4 enhancement on SICM images were MFFPs. Therefore, we thought that when focal pancreatic mass shows incomplete or smooth complete obstruction of common bile duct or pancreatic duct and its signal intensity is equal to or higher than that of the spleen, characterization of the enhancement pattern by adding SICM for the pancreatic mass would be useful to lessen the probability of PDAC.

In this study, we used CTA, which is a non-linear and non-parametric substitute of linear models for categorization. The CTA helps identify and interpret complex interactions, whereas other multivariate analysis can only manage interactions predetermined by the analyst. The CTA uses most significant predictor variables for classification tree. In these tree structures, each interior node corresponds to one of the predictor variables. Leaves represent class labels of the outcome variable and branches represent conjunctions of features that lead to those class labels. CTA provide optimal cut-off points for variables, thus it can be simple to use in decision-making and similar to algorithms used in clinical guidelines. Also, several similar models have been shown to be an efficient tool for differentiation benign from malignant tumour or identifying of high risk group of some disease [33–35].

This study had limitations. First, as it was a retrospective study, there was an unavoidable selection bias. Second, not all

MFFP were surgically resected, and the correlation between histopathological findings and MR features of the lesions was not performed. Third, a relatively small number of study patients with MFFP compared with those with PDAC was included because of the rarity of the disease. Fourth, SICM for MR images and CTA model have been not used for the differentiation of MFFP from PDAC so far. The qualitative evaluation of SICM and determination of reference point for the pancreas would be reader dependent and could be difficult to standardize and reproduce. Also, acquisition of SCIM could be limited due to motion artefact. In addition, in this study, categorization of SCIM was performed in consensus and not by independent reviewers, and interreader agreement was not assessed. Therefore, we think that a sophisticated prospective study would be required to assess the incremental benefits of adding SICM to dynamic MR imaging to differentiate MFFP from PDAC. Furthermore, validating the CTA model in different study populations would be required to demonstrate whether it can be generalized to other populations.

In conclusion, the characterization of enhancement pattern for pancreatic lesions on contrast-enhanced MR images with adding SICM would be helpful to differentiate MFFP from PDAC.

Acknowledgments The scientific guarantor of this publication is Won Jae Lee, the head of radiology department. The authors of this manuscript declare no relationships with any companies, whose products or services may be related to the subject matter of the article. The authors state that this work has not received any funding. One of the authors has significant statistical expertise, Kyunga Kim. Institutional review board approval was obtained. Written informed consent was waived by the Institutional review board. No study subjects or cohorts have been previously reported

References

- Sugiyama Y, Fujinaga Y, Kadoya M et al (2012) Characteristic magnetic resonance features of focal autoimmune pancreatitis useful for differentiation from pancreatic cancer. *Jpn J Radiol* 30:296–309
- Hur BY, Lee JM, Lee JE et al (2012) Magnetic resonance imaging findings of the mass-forming type of autoimmune pancreatitis: Comparison with pancreatic adenocarcinoma. *J Magn Reson Imaging* 36:188–197
- Servais A-M, Pestieau SR, Detry O et al (2001) Autoimmune pancreatitis mimicking cancer of the head of pancreas: report of two cases. *Acta Gastroenterol Belg* 64:227–230
- Hardacre JM, Iacobuzio-Donahue CA, Sohn TA et al (2003) Results of pancreaticoduodenectomy for lymphoplasmacytic sclerosing pancreatitis. *Ann Surg* 237:853–859
- Abraham SC, Wilentz RE, Yeo CJ et al (2003) Pancreaticoduodenectomy (Whipple resections) in patients without malignancy: Are they All Chronic Pancreatitis? *Am J Surg Pathol* 27:110–120
- Kennedy T, Preczewski L, Stocker SJ et al (2006) Incidence of benign inflammatory disease in patients undergoing Whipple procedure for clinically suspected carcinoma: a single-institution experience. *Am J Surg* 191:437–441
- Rasheed ZA (2012) Pathology of pancreatic stroma in PDAC. In : Grippo PJ, Munshi HG (eds) *Pancreatic Cancer and Tumor Microenvironment* Trivandrum (India), Transworld Research Network. Available via <http://www.ncbi.nlm.nih.gov/books/NBK98933/>
- Apte M, Park S, Phillips P et al (2004) Desmoplastic reaction in pancreatic cancer: role of pancreatic stellate cells. *Pancreas* 29:179–187
- Korc M (2007) Pancreatic cancer-associated stroma production. *Am J Surg* 194:S84–S86
- Kim SA, Lee JM, Lee KB et al (2011) Intrahepatic mass-forming cholangiocarcinomas: enhancement patterns at multiphasic CT, with special emphasis on arterial enhancement pattern—correlation with clinicopathologic findings. *Radiology* 260:148–157
- Chari ST, Kloeppel G, Zhang L et al (2010) Histopathologic and clinical subtypes of autoimmune pancreatitis: the Honolulu consensus document. *Pancreatol* 10:664–672
- Shimosegawa T, Chari ST, Frulloni L et al (2011) International consensus diagnostic criteria for autoimmune pancreatitis: guidelines of the International Association of Pancreatology. *Pancreas* 40:352–358
- Haradome H, Grazioli L, Tsunoo M et al (2010) Can MR fluoroscopic triggering technique and slow rate injection provide appropriate arterial phase images with reducing artifacts on gadoxetic acid-DTPA (Gd-EOB-DTPA)-enhanced hepatic MR imaging? *J Magn Reson Imaging* 32:334–340
- Nitta T, Mitsuhashi T, Hatanaka Y, Hirano S, Matsuno Y (2013) Pancreatic ductal adenocarcinomas with multiple large cystic structures: A clinicopathologic and immunohistochemical study of seven cases. *Pancreatol* 13:401–408
- Kosmahl M, Pauser U, Anlauf M, Klöppel G (2005) Pancreatic ductal adenocarcinomas with cystic features: neither rare nor uniform. *Mod Pathol* 18:1157–1164
- Kim HJ, Kim YK, Jeong WK, Lee WJ, Choi D (2015) Pancreatic duct “Icicle sign” on MRI for distinguishing autoimmune pancreatitis from pancreatic ductal adenocarcinoma in the proximal pancreas. *Eur Radiol* 25:1551–1560
- Fattahi R, Balci NC, Perman WH et al (2009) Pancreatic diffusion-weighted imaging (DWI): comparison between mass-forming focal pancreatitis (FP), pancreatic cancer (PC), and normal pancreas. *J Magn Reson Imaging* 29:350–356
- Sun G-F, Zuo C-J, Shao C-W, Wang J-H, Zhang J (2013) Focal autoimmune pancreatitis: radiological characteristics help to distinguish from pancreatic cancer. *World J Gastroenterol* 19:3634–3641
- Negrelli R, Manfredi R, Pedrinolla B et al (2015) Pancreatic duct abnormalities in focal autoimmune pancreatitis: MR/MRCP imaging findings. *Eur Radiol* 25:359–367
- Park MJ, Kim YK, Choi S-y, Rhim H, Lee WJ, Choi D (2014) Preoperative detection of small pancreatic carcinoma: value of adding diffusion-weighted imaging to conventional MR imaging for improving confidence level. *Radiology* 273:433–443
- Breiman L (2001) Random forests. *Mach Learn* 45:5–32
- Ichikawa T, Sou H, Araki T et al (2001) Duct-penetrating sign at MRCP: usefulness for differentiating inflammatory pancreatic mass from pancreatic carcinomas 1. *Radiology* 221:107–116
- Carbognini G, Girardi V, Biasiutti C et al (2009) Autoimmune pancreatitis: imaging findings on contrast-enhanced MR, MRCP and dynamic secretin-enhanced MRCP. *Radiol Med* 114:1214–1231
- Furuhashi N, Suzuki K, Sakurai Y, Ikeda M, Kawai Y, Naganawa S (2015) Differentiation of focal-type autoimmune pancreatitis from pancreatic carcinoma: assessment by multiphase contrast-enhanced CT. *Eur Radiol* 25:1366–1374
- Gangi S, Fletcher J, Nathan MA et al (2004) Time interval between abnormalities seen on CT and the clinical diagnosis of pancreatic

- cancer: retrospective review of CT scans obtained before diagnosis. *AJR Am J Roentgenol* 182:897–903
26. Kamisawa T, Notohara K, Shimosegawa T (2010) Two clinicopathologic subtypes of autoimmune pancreatitis: LPSP and IDCP. *Gastroenterology* 139:22–25
 27. Lee SS, Byun JH, Park BJ et al (2008) Quantitative analysis of diffusion-weighted magnetic resonance imaging of the pancreas: Usefulness in characterizing solid pancreatic masses. *J Magn Reson Imaging* 28:928–936
 28. Huang WC, Sheng J, Chen SY, Lu JP (2011) Differentiation between pancreatic carcinoma and mass-forming chronic pancreatitis: Usefulness of high b value diffusion-weighted imaging. *J Dig Dis* 12:401–408
 29. Barral M, Taouli B, Guiu B et al (2014) Diffusion-weighted MR imaging of the pancreas: current status and recommendations. *Radiology* 274:45–63
 30. Klau M, Lemke A, Grünberg K et al (2011) Intravoxel incoherent motion MRI for the differentiation between mass forming chronic pancreatitis and pancreatic carcinoma. *Invest Radiol* 46:57–63
 31. Kang KM, Lee JM, Yoon JH, Kiefer B, Han JK, Choi BI (2014) Intravoxel incoherent motion diffusion-weighted MR imaging for characterization of focal pancreatic lesions. *Radiology* 270:444–453
 32. Swords DS, Mone MC, Zhang C, Presson AP, Mulvihill SJ, Scaife CL (2015) Initial misdiagnosis of proximal pancreatic adenocarcinoma is associated with delay in diagnosis and advanced stage at presentation. *J Gastrointest Surg* 19:1813–1821
 33. El Malki HO, El Mejdoubi Y, Souadka A et al (2010) Predictive model of biliocystic communication in liver hydatid cysts using classification and regression tree analysis. *BMC Surg*. doi:10.1186/1471-2482-10-16
 34. Thomassin-Naggara I, Toussaint I, Perrot N et al (2011) Characterization of complex adnexal masses: value of adding perfusion-and diffusion-weighted MR imaging to conventional MR imaging. *Radiology* 258:793–803
 35. Nunes LW, Schnall MD, Orel SG (2001) Update of breast MR imaging architectural interpretation model 1. *Radiology* 219:484–494